Soil Moisture Mapping Using Combined Active/Passive Microwave Observations Over the East of the Netherlands

Rogier van der Velde, Mhd. Suhyb Salama, Omar Ali Eweys, Jun Wen, and Qiang Wang

***Abstract*—A coarse resolution soil moisture product is downscaled to 1, 5, and 10 km using synthetic aperture radar (SAR) observations acquired over the east of the Netherlands. The combination of phased array L-band SAR (PALSAR) backscatter and VUA-NASA C-band Advanced Microwave Scanning Radiometer-Earth Observing System (AMSR-E) soil moisture product is adopted to mimic the radar/radiometer setup as will be available from NASA's soil moisture active passive (SMAP) mission. The validation of retrievals is based on measurements collected by a sparse network of 20 stations distributed across 50 $\times$ 75 km study area selected as one of the key validation sites for the SMAP soil moisture products. Reasonable agreements between the measurements and soil moisture retrieved at 1-, 5-, and 10-km resolution are found that lead to coefficients of determination of 0.37, 0.36, and 0.36, respectively. The retrievals, however, severely overestimate the measured soil moisture, which is attributed to the well-known positive bias of the selected AMSR-E product. After bias-correction, root mean squared differences reach as low as $0.046\ \mathrm{m}^3\ \mathrm{m}^{-3}$ for individual locations and are 0.067, 0.068, and $0.069\ \mathrm{m}^3\ \mathrm{m}^{-3}$ on average for the soil moisture retrieved at 1-, 5-, and 10-km resolutions, respectively. These error levels do not satisfy SMAP's targeted accuracy of $0.04\ \mathrm{m}^3\ \mathrm{m}^{-3}$, but the radar/radiometer setup as well as the characterization of the soil moisture conditions representative are not optimal. On the other hand, it is demonstrated that the sequence of soil moisture maps does capture valuable hydrological and hydrometeorological information.**

***Index Terms*—Advanced Microwave Scanning Radiometer-Earth Observing System (AMSR-E), combined active/passive microwave, phased array L-band synthetic aperture radar (PALSAR) scanning SAR (ScanSAR), soil moisture.**

I. Introduction

SOIL MOISTURE as a land state variable plays an important role in various components of the water and energy cycle, such as evapotranspiration, groundwater recharge, and surface runoff. Consequently, reliable soil moisture information following from comprehensive monitoring programs may assist in quantifying the exchanges of water, energy, and carbon fluxes between land and atmosphere. *In situ* soil moisture measurements are labor intensive and site-specific. Yet, frequent spatial soil moisture distributions are needed because of its variability in nature (i.e., [15]). Remotely sensed soil moisture products have the potential of augmenting sparsely distributed measurements of soil moisture from *in situ* networks [32]. Microwave observations have received most attention from the community because of its sensitivity to soil moisture and unique ability to return information on media (atmosphere, vegetation, and soil) that are opaque to the much shorter optical and thermal wavelengths [44].

L-band radiometry is considered to be the most appropriate technique for soil moisture mapping because of its favorable signal-to-noise ratio (i.e., [5], [19], [33], and [40]). The European Space Agency (ESA) as well as National Aeronautics and Space Administration (NASA) have, therefore, supported formulating space missions carrying L-band radiometers for soil moisture monitoring purposes. This has resulted in the launch of the ESA's soil moisture and ocean salinity (SMOS, [23]) mission in 2009 and approval of the NASA's soil moisture active/passive (SMAP, [14]) mission for launch in late 2014. The L-band passive microwave instruments onboard both SMOS and SMAP satellites enable global soil moisture monitoring at a spatial resolution of several tens of kilometers. The resulting data products are expected to contribute to science and applications at the meteorological space and time scales. For applications associated with hydrometeorology, hydrology, and agriculture, however, more detailed spatial information is needed. Downscaling of the coarse resolution passive microwave-based soil moisture products to a higher spatial resolution would, therefore, greatly enhance their applicability.

Various studies have explored the utilization of optical and thermal observations for disaggregation of the coarse resolution data products. For instance, Chauhan *et al.* [6] employed the relationship among vegetation index, surface temperature, and soil moisture for disentangling subpixel information from passive microwave observations. With the launch of SMOS this approach has received more attention. Both Merlin *et al.* [27], [28] and Piles *et al.* [38] have reported on the use of MODerate resolution Imaging Spectrometer (MODIS) optical/thermal observations for downscaling SMOS soil moisture over the calibration/validation (Cal/Val) study area in Australia. Merlin *et al.* [27] concluded, however, that the performance of this approach is highly dependent on the season as the coupling

Manuscript received April 20, 2014; revised July 08, 2014; accepted August 18, 2014. This work was supported by the Chinese Academy of Sciences Fellowship for Young International Scientists under Grant 2012Y1ZA0013.

R. van der Velde, M. S. Salama, O. A. Eweys, and Q. Wang are with the Faculty of Geo-Information Science and Earth Observation, University of Twente, 7500 AE Enschede, The Netherlands (e-mail: r.vandervelde@utwente.nl).

J. Wen is with the Cold and Arid Regions Environmental and Engineering Research Institute (CAREERI/CAS), Lanzhou 730000, China.

Color versions of one or more of the figures in this paper are available online at http://ieeexplore.ieee.org.

Digital Object Identifier 10.1109/JSTARS.2014.2353692

of the soil moisture to surface temperature is weak during the cold and wet episodes.

An alternative approach for downscaling the coarse resolution passive microwave-based soil moisture products is through the combination with high resolution active microwave observations that can be acquired via the synthetic aperture radar (SAR) technique at spatial resolutions up to several meters from space. Active microwave observations outweigh the optical/thermal observations due to their sensitivity to soil moisture over the complete dynamic range and continuous availability for land under all weather conditions. Chauhan *et al.* [7] and O'Neill *et al.* [34] were among the first to investigate the synergistic use of active and passive microwave observations via a physically based radiative transfer approach applied to data collected at field-scale with a truck-mounted radar and radiometer.

Njoku *et al.* [32] proposed a more pragmatic approach based on change detection for the retrieval of soil moisture from passive/active L-band system (PALS) data collected during the Southern Great Plains Experiment in 1999 (SGP99). This change detection approach is based on the near linear relationship between radar backscatter (σ^{o}) and volumetric soil moisture (i.e., [12] and [33]) and thereby assumes time-invariant surface roughness and vegetation effects. Expanded upon the work of Njoku *et al.*, Narayan *et al.* [31] presented a change detection algorithm for combination of the PALS and airborne SAR (AIRSAR) from the Soil Moisture Experiment 2002 (SMEX02) campaign conducted in an agricultural setting. With the SMAP mission entering its formulation phase, Piles *et al.* [37] continued the development of this approach by applying the algorithm within the synthetic setup of an observation system simulation experiment (OSSE), which provided a better quantification of retrieval uncertainties. Das *et al.* [9] extended the method further, which was proposed as baseline algorithm for the SMAP 9-km combined active/passive soil moisture product (SMAP A/P). The major contribution is that this algorithm provides an absolute soil moisture content rather than the relative measure supplied by its predecessors. A disadvantage is, however, that the accuracy at the target resolution highly depends on the passive microwave soil moisture retrievals. Recently, a modified version of the baseline algorithm for the SMAP A/P product has, therefore, been reported in [10], whereby the focus is on using the σ^{o} for downscaling brightness temperatures (T_{b}s) from which soil moisture is retrieved rather than for directly downscaling the radiometer soil moisture product. The challenge of this procedure lies in the procurement of reliable ancillary data (e.g., temperature, vegetation water content) needed for soil moisture retrieval from T_{b}s across the globe with a high spatial resolution.

We apply in this paper the algorithm described in [9] to a soil moisture product derived from the C-band passive microwave data observed by the Advanced Microwave Scanning Radiometer-Earth Observing System (AMSR-E) and corresponding L-band σ^{o} data from the Phased Array L-band Synthetic Aperture Radar (PALSAR). The available data set consists of 48 AMSR-E soil moisture-PALSAR σ^{o} pairs acquired over the eastern part of the Netherlands (Twente) in 2008 and 2010 for the period from May to November. The PALSAR observations have been collected in the scanning SAR (ScanSAR) mode at a 100-m spatial resolution. This allows us to generate the soil moisture maps at resolutions higher than 9 km selected for the SMAP A/P product. For this study, the combined soil moisture maps are produced with spatial resolutions of 1, 5, and 10 km. The accuracy of these products is assessed through comparison against *in situ* measurements collected by a network of 20 individual stations located within the Twente region selected as a key site for the global Cal/Val activities of SMAP data products.

It should, however, be noted that the L-band passive microwave observations provided by, for instance, the SMOS satellite would be preferred for testing the capabilities of the combined radar/radiometer setup for soil moisture monitoring as will be available on SMAP. However, the presence of radio frequency interference (RFI) in the SMOS observations over Twente causes its soil moisture product to be unreliable in this region [11]. Hence, we have chosen to use the C-band AMSR-E product instead. It is expected, however, that this will have a limited impact on the main results and conclusions.

II. Study Area and Data Sets

A. Description of the Study Area

The selected study area is the Twente region (Fig. 1) located in the eastern part of the Netherlands (52.00–52.50 N latitude and 6.25–7.00 E longitude). The topography in Twente is almost flat with elevations varying from -3 to 50 m above sea level. Land cover is heterogeneous and consists of pastures, agricultural, forested, and urban areas. Lying in the temperate zone, it experiences mild summers and mild wet winters. The monthly mean air temperatures range from 3°C in January to approximately 17°C in July. Rain events are evenly distributed throughout the year resulting in a mean annual sum of about 765 mm. Twente region has four main soil types, including sandy soils, loamy soils, manmade sandy thick earth soils, and peat soils covered by a layer of peat or sand, whereby sand and loamy sand are dominant near the surface.

B. In Situ Measurements

Since September 2009, the study area is equipped with a ground-based soil moisture/temperature monitoring network that consists of twenty stations where soil moisture and temperature are measured every 15 min at nominal depths of 5, 10, 20, 40, and 80 cm. The sites cover an area of 50×40 km in which one is installed in forested area, 16 are located in grass dominated pastures and 3 in corn fields. The measurements are performed with EC-TM ECH2O probes, which use a capacitance technique for measuring the dielectric permittivity of the soil. The dielectric permittivity is converted into volumetric units ($\mathrm{m}^3\,\mathrm{m}^{-3}$) using a soil-specific calibration function developed from laboratory measurements that leads to an estimated accuracy of $0.023\ \mathrm{m}^3\,\mathrm{m}^{-3}$. Further information on development of the soil monitoring network can be found in [11] and at http://www.itc.nl/library/papers_2011/scie/dente_twe.pdf.

Rainfall measurements are available from the water board district called "Vechtstromen." The water board operates 18 automated rain gauge stations installed in the so-called

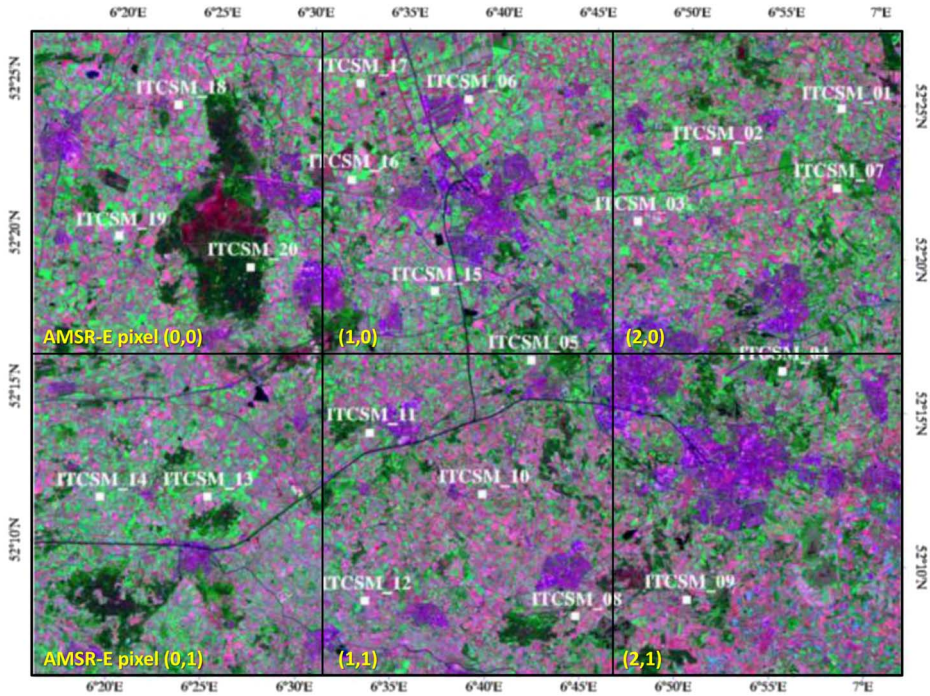

Fig. 1. Landsat 5 TM image (RGB: band 7, band 4, and band 2) acquired on June 27, 2010 of the Twente region with the labels of soil moisture/temperature stations shown in white and the locations indicated by white squares. The approximate extents of the AMSR-E pixels are shown as well.

"English setup" at the water treatment plants within the district. These stations consist of tipping buckets with a 0.1-mm resolution and the capability of recording measurements every 20 min. For this study, the 20-min values are summed to daily amounts.

Fig. 2 shows the top 5 cm soil moisture measured in 2010 at two representative pastures (ITCSM01 & -11) and a corn field (ITCSM07) along with rainfall amounts collected at the nearest water treatment plant. The plots illustrate the soil moisture dynamics that are typical for this part of the Netherlands. In general, winters are wet due to a low evaporative demand and temporally evenly distributed rainfall. From the onset of spring till autumn, larger temporal variations are noted because dry spells often end with a series of intensive rain events. In this context, 2010 was an extreme dry year as the months May, June, July, and the first half of August received less rain than expected, whereas only in the second half of August more than 200 mm was collected in some parts of the district. This led to severe floods across the entire region. The soil moisture fluctuations in response to these rain events provide confidence in the reliability of the measurements.

C. PALSAR System and Data Processing

The PALSAR instrument onboard the Advanced Land Observing Satellite (ALOS) was a L-band (1.27 GHz) SAR system capable of operating in various modes with different polarizations, spatial resolutions (10–100 m) and image swaths (30–350 km) with revisit times of 46 to 2 days. For this study, 48 PALSAR acquisitions collected in the HH polarization and ScanSAR mode are available. In the ScanSAR mode, PALSAR collected single polarized σ^{o} data over a 350-km swath width processed to spatial resolution of 100 m with a nominal revisit of 2–5 days. Four PALSAR acquisitions were collected from an ascending orbit around 21:30 UTC (22:30 local time) and the other data sets were obtained from a descending orbit at a nominal UTC time of 10:30 (11:30 local time). The radiometric accuracy of PALSAR data is reported to be better than 1 dB [41] and Table I gives additional technical information on the PALSAR ScanSAR mode.

The ESA provided the PALSAR data sets as ellipsoid geocoded (level 1.5) products listed in Table II. These PALSAR ScanSAR products are processed using the Next ESA SAR Toolbox (NEST) version 4C-1.1 and calibrated to σ^{o} values after removal of the antenna pattern. The speckle noise inherent to the coherent sensing technique of SAR systems is suppressed via application of a nonadaptive median filter with a kernel of 5×5 pixels in analogy with, for instance, [43] and [46]. The study area is extracted from the speckle filtered PALSAR σ^{o} products and these subsets are automatically coregistered.

D. LPRM AMSR-E Soil Moisture Products

The selected AMSR-E soil moisture product is the one produced with the Land Parameter Retrieval Model (LPRM) described in [35] and [36] applied to the C-band (6.925 GHz) brightness temperatures (T_{b}). The LPRM algorithm uses a radiative transfer approach to separate microwaves emission contributions from soil and vegetation. The advantage of the LPRM concept is that little additional information is needed to account for vegetation effects.

The gridded level-3 product has been used for this study, which is resampled to a 0.25-degree spatial resolution from the coarser resolution LPRM AMSR-E retrievals (56 km at C-band). AMSR-E collected each day 15 orbits with a revisit time of 1–2 day(s) depending on the geographic

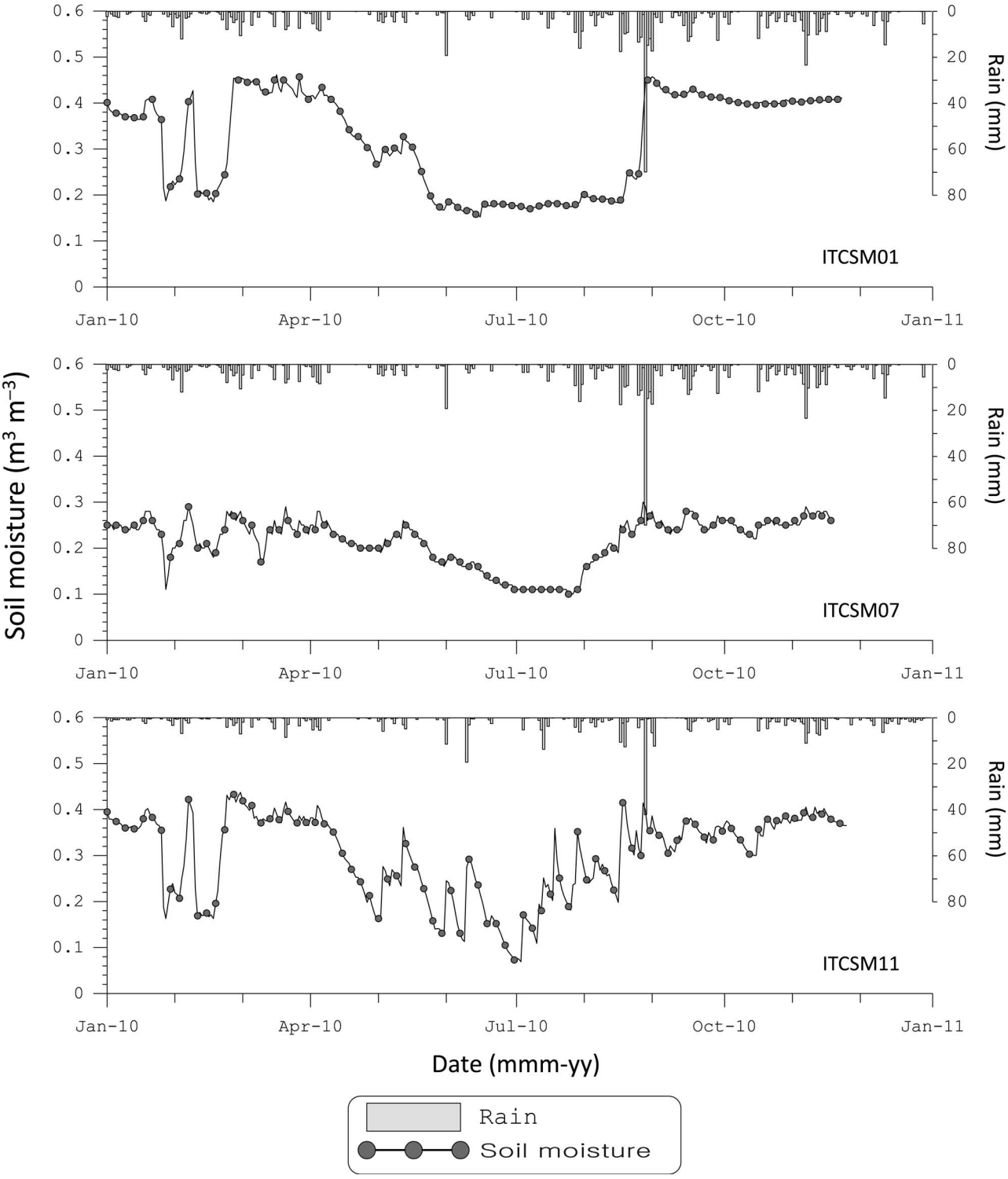

Fig. 2. Five centimeter soil moisture measured at stations located in two pastures (ITCSM01 & -11) and a corn field (ITCSM07), and rain amounts collected at nearest station operated by the water board at water treatment plants.

location. The descending AMSR-E soil moisture product (obtained at 01:30 A.M. local time) is chosen because various studies (i.e., [13], [20], and [42]) have shown through comparison against *in situ* measurements that those retrievals are more reliable. The AMSR-E LPRM data are obtained from ftp://hydro1.sci.gsfc.nasa.gov/data/s4pa/WAOB/LPRM_AMSRE_D_SOILM3.002/.

III. Retrieval Method

A. Downscaling Approach

The method described in [9] uses high-resolution active microwave observations to downscale the coarse passive microwave soil moisture retrievals. To this aim, a linear relationship is assumed between σ^{o} and the soil moisture retrieved

TABLE I
PALSAR SCANSAR MODE SENSING CHARACTERISTICS

Mode	ScanSAR (WB1)
Central frequency	1.27 GHz
Polarization	HH
Spatial resolution	100 m
Incidence angle	18°–43.3°
Orbit acquisition	Ascending/descending
Overpass time	Ascending: around 10:30 P.M. Descending: around 10:30 A.M.
S/N	< -23 dB

from passive microwave observations. Before downscaling, the high resolution σ^{o} in $\mathrm{m}^2\,\mathrm{m}^{-2}$ units is aggregated to an intermediate resolution and subsequently converted into dB. This step is performed to further suppress the effects of speckle noise on the soil moisture product. Fig. 3 illustrates this downscaling procedure, which can mathematically be expressed as

$$\theta_m = \theta_c + \beta_c * (\sigma^{\mathrm{o}}_{\mathrm{m}} - \sigma^{\mathrm{o}}_{\mathrm{c}}) \tag{1}$$

where θ is the volumetric soil moisture ($\mathrm{m}^3\,\mathrm{m}^{-3}$), σ^{o} is the backscatter (dB), β is an empirical parameter describing soil moisture sensitivity of σ^{o} ($\mathrm{m}^3\ \mathrm{m}^{-3}\ \mathrm{dB}^{-1}$) and subscripts m and c indicate that the variable is representative for either the medium or coarse spatial resolution, respectively.

The parameter β is obtained at the coarse resolution from the relationship between the θ and σ^{o}. Through application of a linear regression to a set of $\theta_c - \sigma^{\mathrm{o}}_{\mathrm{c}}$ matchups, the β_{c} is defined for each coarse resolution grid cell as

$$\theta_c = \alpha_c + \beta_c * \sigma^{\mathrm{o}}_{\mathrm{c}} \tag{2}$$

where α_c is an empirical calibration parameter depending on vegetation cover and soil surface roughness ($\mathrm{m}^3\,\mathrm{m}^{-3}$). The β_{c} and α_{c} are taken as parameters independent of spatial scale and, thus, the heterogeneity within a coarse grid cell is ignored. The parameters are ideally derived from $\sigma^{\mathrm{o}}_{\mathrm{c}}$ data collected over a period in which little changes in the effects of vegetation occur. The complete set of 48 AMSR-E soil moisture-PALSAR σ^{o} pairs is employed for the determining β_{c} in this study and, thereby, we assume that the vegetation effects on σ^{o} remain constant. The validity of this assumption is evaluated in Section VI-B.

B. View Angle Correction

PALSAR ScanSAR data are collected at view angles ranging from 18° to 43.4°. Correction for σ^{o} differences due to this angular variability is needed, which is often done by normalizing the observations toward a reference angle. Various data driven procedures (e.g., [49] and [26]) have been developed that are suitable when the dielectric properties of the observed soil–vegetation system either remain constant or cover an evenly distributed range to avoid a bias in the applied corrections toward the data set.

The most commonly adopted semiempirical method is the cosine correction (i.e., [30]) whereby the σ^{o} is normalized toward a reference angle using

$$\sigma^{\mathrm{o}}_{\mathrm{ref}} = \sigma^{\mathrm{o}} \frac{\cos^n(\theta_{\mathrm{ref}})}{\cos^n(\theta_{\mathrm{v}})} \tag{3}$$

where θ_{v} is the view angle (degrees), $\sigma^{\mathrm{o}}_{\mathrm{ref}}$ is the backscatter normalized to a reference angle, θ_{ref} ($\mathrm{m}^2\mathrm{m}^{-2}$), and n depends on the type of scattering and ultimately the land cover characteristics (–). The power n taken equal to 1 applies when volume scattering is dominant and σ^{o} varies only with proportion to the projected area (e.g., [1]). Forests and snowpack typically exhibit such behavior [51]. When reradiation of the incident energy follows the cosine law, instead of being isotropic, n should be taken equal to 2, which is in essence an application of Lambert's law for optics [44]. This type of behavior can be observed over rough surfaces in the mid-range of angles and has been applied with reasonable success to C- and L-band SAR data by Lievens *et al.* [25] and Van der Velde *et al.* [45]. Ardila *et al.* [3] specifically investigated the magnitude of n by fitting the view angle and PALSAR HH polarized σ^{o} observed over tropical forest dominated areas and found n values varying from 0.24 for forests to 3.36 for savanna. As such, previous research has shown that the theoretical assignment of $n = 1$ and $n = 2$ applies when the target area behaves as or approaches the behavior of a volume scatterer.

The angular behavior of the HH polarized PALSAR σ^{o} data over the study area is evaluated by normalizing σ^{o} observed over the stations of the Twente soil moisture/temperature monitoring network to a 30° reference angle. The n is taken as the value for which the slope between $\sigma^{\mathrm{o}}_{\mathrm{ref}}$ and θ_{v} is zero, whereby a negative n is considered invalid. Table III lists the values for the 20 stations that range from 0.00 to 2.21. The n values are on average 0.70 for the 16 pastures, 1.36 for 3 corn fields and 0.73 for the forest. The angular responses deduced from the σ^{o} observations of the three land covers (pasture, corn, and forest) are surprisingly comparable to each other. On the other hand, this can be argued for because the agricultural fields in the study area are mixed in the landscape with tree lines of variable sizes and have dimensions in the same order of magnitude as the PALSAR spatial resolution (100 m). As such, the angular behavior of a volume scatterer may be justifiable for the study area. In the following analyses, the PALSAR σ^{o} normalized with $n = 1$ is employed because it appears to be most appropriate for this data set. The impact of this assumption on the soil moisture retrievals is discussed in Section VI-A.

IV. PALSAR AND AMSR-E DATA ANALYSIS

The key to a successful application of the retrieval method is that 1) σ^{o} is sensitive to soil moisture, 2) passive microwave soil moisture product is accurate, and 3) σ^{o} and passive microwave soil moisture product are positively correlated to each other. In the text below, these three items are discussed through comparisons of the PALSAR σ^{o} and the AMSR-E LPRM product against *in situ* measurements and each other.

TABLE II
LIST OF PALSAR SCANSAR DATA SETS USED FOR THE INVESTIGATION

Index	Date	Overpass time*	Orbit	Orbital Acquisition	Index	Date	Overpass time*	Orbit	Orbital Acquisition
1	23/05/2008	10:25	12404	Descending	25	14/07/2010	10:29	23811	Descending
2	09/06/2008	10:27	12652	Descending	26	21/07/2010	10:18	23913	Descending
3	21/06/2008	10:22	12827	Descending	27	26/07/2010	10:24	23986	Descending
4	03/07/2008	10:18	13002	Descending	28	31/07/2010	10:31	24059	Descending
5	08/07/2008	10:24	13075	Descending	29	02/08/2010	10:13	24088	Descending
6	20/07/2008	10:20	13250	Descending	30	07/08/2010	10:20	24161	Descending
7	18/08/2008	10:18	13673	Descending	31	12/08/2010	10:26	24234	Descending
8	23/08/2008	10:25	13746	Descending	32	19/08/2010	10:15	24336	Descending
9	04/09/2008	10:21	13921	Descending	33	24/08/2010	10:22	24409	Descending
10	21/09/2008	10:23	14169	Descending	34	29/08/2010	10:28	24482	Descending
11	03/10/2008	10:19	14344	Descending	35	08/09/2010	21:51	24635	Ascending
12	08/10/2008	10:26	14417	Descending	36	15/09/2010	10:30	24730	Descending
13	25/10/2008	10:28	14665	Descending	37	27/09/2010	10:25	24905	Descending
14	01/11/2008	10:18	14767	Descending	38	04/10/2010	10:15	25007	Descending
15	06/11/2008	10:25	14840	Descending	39	14/10/2010	10:27	25153	Descending
16	18/11/2008	10:21	15015	Descending	40	26/10/2010	10:23	25328	Descending
17	23/11/2008	10:27	15088	Descending	41	05/11/2010	21:46	25481	Ascending
18	24/05/2010	10:23	23067	Descending	42	12/11/2010	10:25	25576	Descending
19	29/05/2010	10:29	23140	Descending	43	19/11/2010	10:14	25678	Descending
20	15/06/2010	10:31	23388	Descending	44	22/11/2010	21:48	25729	Ascending
21	17/06/2010	10:14	23417	Descending	45	24/11/2010	10:20	25751	Descending
22	27/06/2010	10:27	23563	Descending	46	29/11/2010	10:27	25824	Descending
23	04/07/2010	10:16	23665	Descending	47	06/12/2010	10:16	25926	Descending
24	09/07/2010	10:22	23738	Descending	48	21/12/2010	21:45	26152	Ascending

*Time shown is in UTC.

A. Backscatter Sensitivity to Soil Moisture

Many studies (i.e., [9], [12], [24], [33]) have previously reported on the near linear relationship between σ° and soil moisture. Fig. 4 shows the normalized PALSAR σ° averaged over a kernel size of 5×5 pixels against the soil moisture measured at two pastures (ITCSM05 and -15), two corn fields (ITCSM07 and -08) and a forest site (ITCSM20) to investigate this relationship for the study area. Indeed, the plots demonstrate the linear dependence of the PALSAR σ° on measured soil moisture for all three land covers.

For both the pastures and corn fields reasonably high coefficients of determination (R^2) are obtained ranging from 0.43 to 0.64, whereby for the pastures a smaller spread in the data points is noted among the fitted regression line than for the corn fields. This is most likely associated with the more intensive farming practices at corn fields that changes the surface roughness and vegetation effects on the PALSAR σ°. Nevertheless, the soil moisture signal detected is appreciable, which can be expected based on previous studies by, for instance, Joseph *et al.* [22]. They found that soil moisture relationship between soil moisture and the HH polarized L-band σ° measured with a truck-mounted scatterometer from view angles of 15°, 35°, and 55° results in R^2 values of 0.74, 0.74, and 0.32, respectively.

Considering the vegetation biomass, it is somewhat surprising to note that the σ° sensitivity to soil moisture, taken as the slope of the linear equations in Fig. 4, is larger for the corn field than for the pastures. Pastures are typically less densely vegetated than corn fields at peak biomass. The explanation for this could be that near the peak corn biomass scattering mechanisms along the soil–vegetation pathways enhances the σ° sensitivity to soil moisture. Indeed, several studies (e.g., [21], [22], and [24]) have provided experimental evidence for a significant soil moisture signal within σ° observations collected over mature corn canopies (vegetation water content > 2.5 kg m^{-2}). On the other hand, a large portion of the year the corn fields lie fallow or crops are not fully developed, whereas the pastures are fully covered by grass throughout the year. This could also explain the larger σ° sensitivity to soil moisture noted. An important implication is that based on the σ° sensitivity to soil moisture alone the radar system needs to measure σ° with noise levels better than 0.48 and 0.61 dB for pastures and corn fields, respectively to achieve 0.04 m^3 m^{-3} error level targeted by soil moisture missions, such as SMAP.

Over the forest site the relationship between σ° and soil moisture is much weaker, which can be explained by the fact that the forest attenuates most of the signals coming from the soil (i.e., [16] and [39]). Also, much higher σ° values are recorded over the forest than over the pastures and corn fields; about -6.0 to -4.0 dB for forest versus a maximum of -5.0 dB for corn. This is expected because forests are typically strong scatterers, whereas sparse to moderately dense vegetation becomes more transparent at the low L-band frequencies. Nevertheless, a clear positive relationship is noted between the PALSAR σ° and measured soil moisture with a fairly small spread among the data points. However, based on the low sensitivity to soil moisture alone, a radar system would be required with an accuracy of 0.20 dB to achieve a soil moisture error better than 0.04 m^3 m^{-3}. On the other hand, soil moisture retrieval over forests is typically not part of satellite mission objectives [14].

B. LPRM AMSR-E Product Validation

In this section, the descending LPRM AMSR-E soil moisture products are validated against *in situ* measurements at two spatial scales for the same dates as the PALSAR observations are

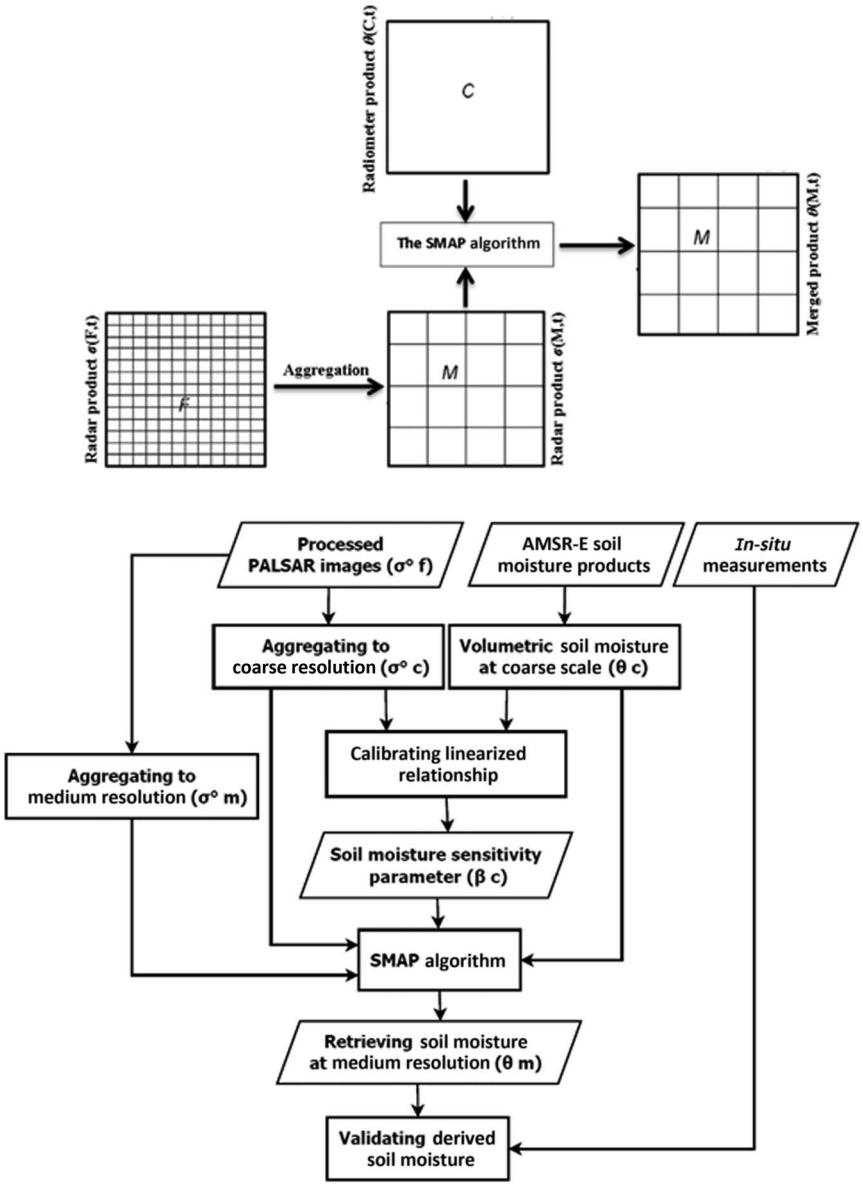

Fig. 3. Grid topology and schematization of the SMAP A/P algorithm for downscaling coarse passive microwave soil moisture with fine σ^{o} (reproduced based on [9]).

available. The satellite products are compared against measurements from individual stations and against soil moisture values obtained through averaging the measurements of all stations within a grid cell. From the matchups, the bias, R^2, root-mean-square difference (RMSD) and mean absolute difference (MAD) are calculated and listed in Table IV. It should be noted that station ITCSM16 is not included in validation because a large part of its measurements were not reliably retrieved from the data loggers.

For both comparisons with individual measurements and grid-cell averaged soil moisture, LPRM AMSR-E product assessment results in R^2 values varying across the range of 0.08–0.64. This finding is comparable to the results reported in [13] and [18] in which LPRM products are compared to *in situ* measurements over various climatological conditions. For instance, Draper *et al.* reported for an Australian study area on Pearson correlation coefficients (r) ranging from 0.67 to 0.92, which is equivalent to R^2 values of 0.45–0.85. The LPRM validation in [18] was conducted for a low vegetated and homogenous area in Mali through making comparison with upscaled *in situ* measurements. They found r (R^2) values of 0.89 (0.79), 0.58 (0.34), and 0.60 (0.36) for a 2 years period.

An examination of Table IV shows, however, that the R^2 values are not as high reported in the literature. This can be argued for because our study area includes significant portions of forested and urbanized areas. On the other hand, the lowest R^2 values are obtained for the AMSR-E pixels for which only two measurement locations are available. Hence, the spatial representation of the reference soil moisture may be an issue as well (see for a review [8]). This is further motivated by the fact that the highest R^2 values are obtained for pixels with the largest number of measurement locations.

TABLE III
VALUES OF n, NEEDED TO NORMALIZE σ^{o} OBSERVATIONS TO A REFERENCE ANGLE USING THE COSINE CORRECTION, DERIVED FROM THE PALSAR-VIEW ANGLE PAIRS OBTAINED OVER THE STATIONS OF THE TWENTE SOIL MOISTURE/TEMPERATURE MONITORING NETWORK STATIONS

Pasture		Corn		Forest	
Station	n[1]	*Station*	*n*	*Station*	*n*
ITCSM01	****	ITCSM07	0.72	ITCSM20	0.73
ITCSM02	1.44	ITCSM08	1.32		
ITCSM03	0.00	ITCSM09	2.06		
ITCSM04	2.21				
ITCSM05	0.63				
ITCSM06	****				
ITCSM10	0.76				
ITCSM11	0.18				
ITCSM12	0.50				
ITCSM13	1.78				
ITCSM14	****				
ITCSM15	0.36				
ITCSM16	1.48				
ITCSM17	0.36				
ITCSM18	0.37				
ITCSM19	1.07				
Mean	0.70		1.36		0.73

[1]Negative values are marked as invalid.

Results from the LPRM validation against individual stations show to our surprise that one of the best agreements is found for the forest site (ITCSM20). The soil moisture dynamics in the sampled forest represents apparently the AMSR-E footprint quite well.

Furthermore, it should be noted that Table IV shows in general high positive biases. The LPRM products typically overestimate the *in situ* measurements by more than 0.18 m^3 m^{-3} on the AMSR-E grid scale, which also explains the large RMSD and MAD values. The large bias is a well-known problem for LPRM AMSR-E products and has previously been identified (e.g., [13], [50]). Evidently, this will have consequences for matchup of combined active/passive microwave soil moisture retrievals and *in situ* measurements.

C. PALSAR Backscatter Versus AMSR-E Soil Moisture

The soil moisture sensitivity parameter (β_{C}) of the selected downscaling approach is determined by fitting a linear equation through data points consisting of, in this case, the LPRM AMSR-E volumetric soil moisture and PALSAR σ^{o} aggregated to the AMSR-E resolution. Then, the slope of the linear equation is taken as β_{C}. Fig. 5 illustrates the relationship between LPRM AMSR-E soil moisture and PALSAR σ^{o}.

From the figure, the slope varies from 0.0293 to 0.0332 $m^3\,m^{-3}\,dB^{-1}$. The small variability observed among the slopes (standard deviation of 0.0014 $m^3\,m^{-3}\,dB^{-1}$) may suggest that land surface heterogeneity does not significantly impact β_{C} when the σ^{o} is aggregated to the coarse passive microwave resolution. The obtained slopes, viz. β_{C}, accommodate a sensitivity of $0.0293-0.0332$ $m^3\,m^{-3}/dB$. This is somewhat better than the σ^{o} sensitivity to soil moisture found at the level of the individual measurement locations, which may suggest on the other hand that β_{C} depends on the spatial scale.

V. COMPARISON AGAINST *IN SITU* MEASUREMENTS

The downscaling method is applied as described in Section III to the LPRM soil moisture-PALSAR σ^{o} pairs to estimate soil moisture at three spatial resolutions, respectively, 1, 5, and 10 km, to evaluate its performance at various spatial scales. In this section, the accuracy of the soil moisture products is assessed by comparing the retrievals against the soil moisture measured at individual stations. As error statistics the bias, R^2, RMSD, and MAD are calculated from the matchups. Table V provides these statistics for the individual stations as well as a summary. This assessment is performed only for the year 2010, because the soil moisture/temperature network is fully operational from 2009 and again ITCSM16 is not included in the analysis.

In general, Table V shows that R^2 values vary from 0.07 (ITCSM13) to 0.61 (ITCSM01) for the soil moisture retrieved at the 1-, 5-, and 10-km resolutions. This R^2 range is comparable to the statistics computed between the LPRM and measured soil moisture to some extent. Although the overall agreement between the retrieved and measured soil moisture improves slightly by downscaling of the LPRM AMSR-E product to a finer resolution, also reductions of the R^2 are noted for eight stations. As an example, a decrease of more than 35% is found for ITCSM11.

Such decrease in the agreement between retrievals and measurements can have several causes. For instance, Van der Velde *et al.* [47] reported on the severity of spatial scale mismatch on the agreement between high resolution retrievals and soil moisture measurements from a single location. Also, the PALSAR σ^{o} aggregated to a 1-km spatial resolution will be more affected by speckle noise than at the coarser 5- and 10-km resolutions. Furthermore, the assumption that β_{C} does not depend on the spatial scale inevitably introduces a larger uncertainty at higher spatial resolution specifically for the selected study areas with a fairly large land cover heterogeneity.

Fig. 6 presents scatter plots for a typical pasture (ITCSM03), corn (ITCSM07), and forest (ITCSM20) sites to illustrate the agreement found between the retrieved and measured soil moisture at the three spatial resolutions. The spread among the data points, R^2, remains at the same level or increases with the spatial resolution for the pasture and corn site, whereas it decreases with the spatial resolution for the forested area. Similarly, the slope of the linear equation fitted through the data points changes with the spatial resolution. A decrease in the slope is noted for the pasture and corn at coarse resolution, while an increase is found for the forest.

This highlights the inherent property of the applied downscaling method. In Section IV, it is shown that for the forest site the PALSAR σ^{o}—soil moisture relationship is well defined, and that the measured and LPRM soil moisture agree with other as well. This combination is needed for a fairly successful application of the selected downscaling approach because for other sites the PALSAR σ^{o}—soil moisture relationship is favorable, but measured-LPRM soil moisture matchup is poor or vice versa. In this context, a more localized formulation of β_{C} may assist in generating more robust combined active/passive microwave soil moisture products.

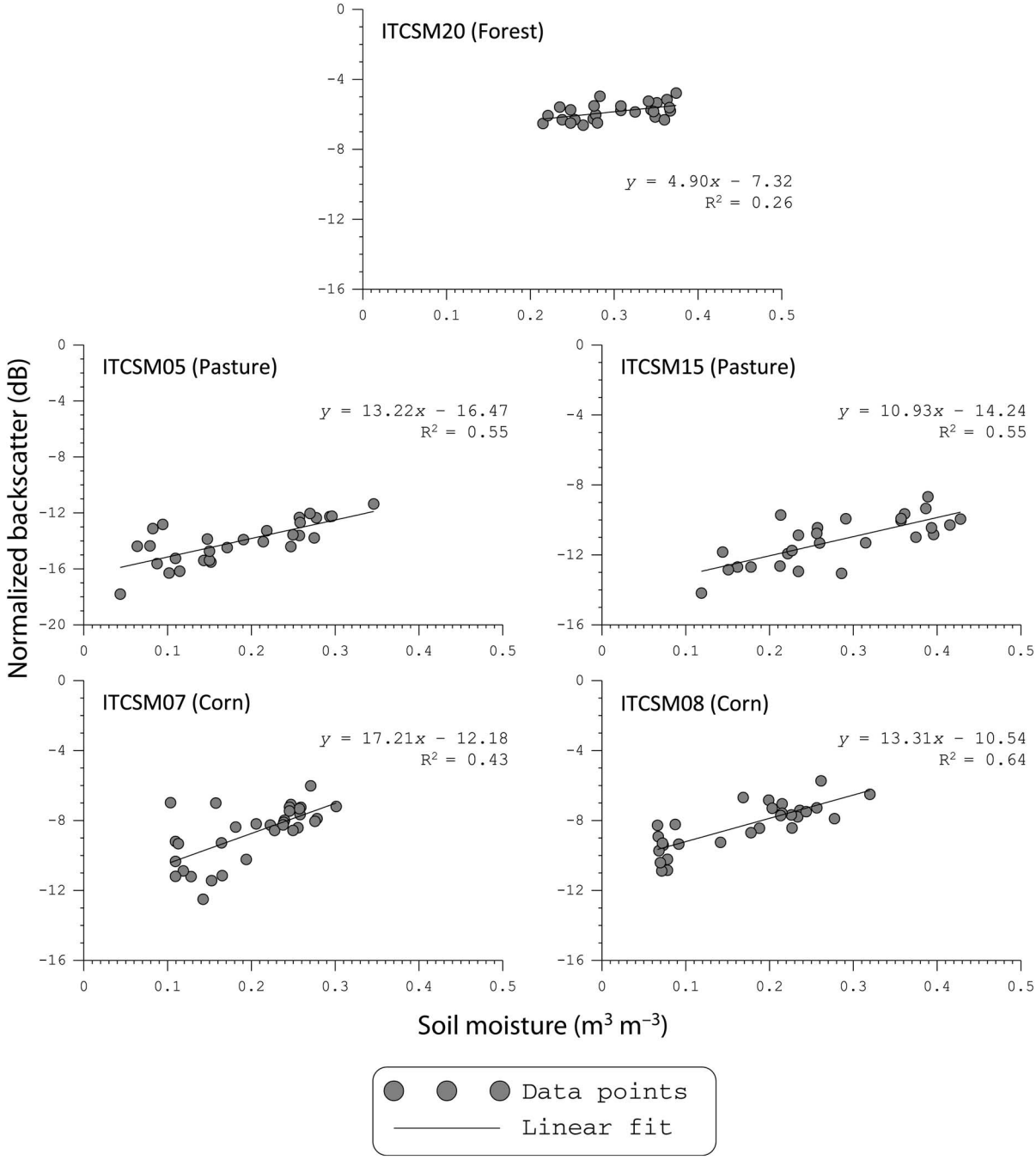

Fig. 4. Normalized PALSAR σ^{o} plotted against the soil moisture measured at stations located in two pastures (ITCSM05 & -15), two corn fields (ITCSM07 & -08), and a forested area (ITCSM20).

Despite the positive relationship found between the retrieved and measured soil moisture, a large overestimation of the measurements is noted of 0.182, 0.180, 0.187 $m^3\,m^{-3}$, on average, for the 1-, 5-, and 10-km products, respectively. This is associated with the fact that the downscaling method relies on the passive microwave soil moisture product as benchmark. In this case, the LPRM AMSR-E product is employed, for which the positive bias toward *in situ* measurements is well-known. This is also confirmed in Section IV for the selected study area. The bias increases also the other error statistics, RMSD and MAD, and assures that the targeted 0.04 $m^3\,m^{-3}$ soil moisture error is not achieved by far.

Under the assumption that the passive microwave soil moisture product is unbiased, a correction is applied to the retrievals by simply subtracting the bias; an approach that is frequently used, e.g., [4]. Using the bias-corrected retrievals the error statistics (RMSD, MAD) are recalculated.

Table VI presents for the individual stations the obtained statistics as well as the mean and standard deviation of the statistics. Clearly, the bias-correction procedure reduces the RMSD as well as the MAD by more than 50%. Additionally, the bias removal suppresses the large variations in the RMSD found for individual stations. For instance, the RMSD range of 0.061–0.293 $m^3\,m^{-3}$ for the 1-km products reduces to

TABLE IV
STATISTICS (R^2, BIAS, RMSD, AND MAD) COMPUTED BETWEEN LPRM AMSR-E SOIL MOISTURE AND MEASUREMENTS OF INDIVIDUAL STATIONS AS WELL AS MEAN VALUES OF ALL MEASUREMENTS AVAILABLE WITHIN AN AMSR-E PIXEL

			Validation against individual stations				Validation against mean soil moisture averaged over the stations within an AMSR–E grid cell				
AMSR–E pixel	Stations	Land Cover	R^2	Bias ($m^3\ m^{-3}$)	RMSD ($m^3\ m^{-3}$)	MAD ($m^3\ m^{-3}$)	R^2	Bias ($m^3\ m^{-3}$)	RMSD ($m^3\ m^{-3}$)	MAD ($m^3\ m^{-3}$)	n (#)
(0,0)	ITCSM18	Pasture	0.39	0.272	0.281	0.253	0.52	0.193	0.201	0.190	3
	ITCSM19	Pasture	0.42	0.192	0.258	0.224					
	ITCSM20	Forest	0.47	0.140	0.197	0.176					
(1,0)	ITCSM05	Pasture	0.29	0.249	0.257	0.241	0.47	0.202	0.222	0.214	4
	ITCSM06	Pasture	0.55	0.207	0.234	0.222					
	ITCSM15	Pasture	0.41	0.123	0.199	0.168					
	ITCSM17	Pasture	0.58	0.311	0.308	0.293					
(2,0)	ITCSM01	Fallow Pasture	0.61	0.134	0.202	0.174	0.56	0.171	0.182	0.171	5
	ITCSM02	Pasture	0.68	0.308	0.310	0.301					
	ITCSM03	Pasture	0.56	0.084	0.144	0.101					
	ITCSM04	Pasture	0.57	0.181	0.211	0.190					
	ITCSM07	Corn Field	0.47	0.207	0.217	0.206					
(0,1)	ITCSM13	Pasture	0.09	0.268	0.278	0.269	0.08	0.178	0.190	0.178	2
	ITCSM14	Pasture	0.12	0.125	0.163	0.078					
(1,1)	ITCSM08	Corn Field	0.26	0.257	0.270	0.255	0.27	0.128	0.140	0.128	4
	ITCSM10	Pasture	0.35	0.103	0.153	0.130					
	ITCSM11	Pasture	0.26	0.147	0.204	0.170					
	ITCSM12	Pasture	0.48	0.270	0.279	0.269					
(2,1)	ITCSM09	Corn Field	0.21	0.209	0.229	0.210	0.21	0.209	0.221	0.209	1

n stands for the number soil moisture measurements available for an AMSR-E pixel.

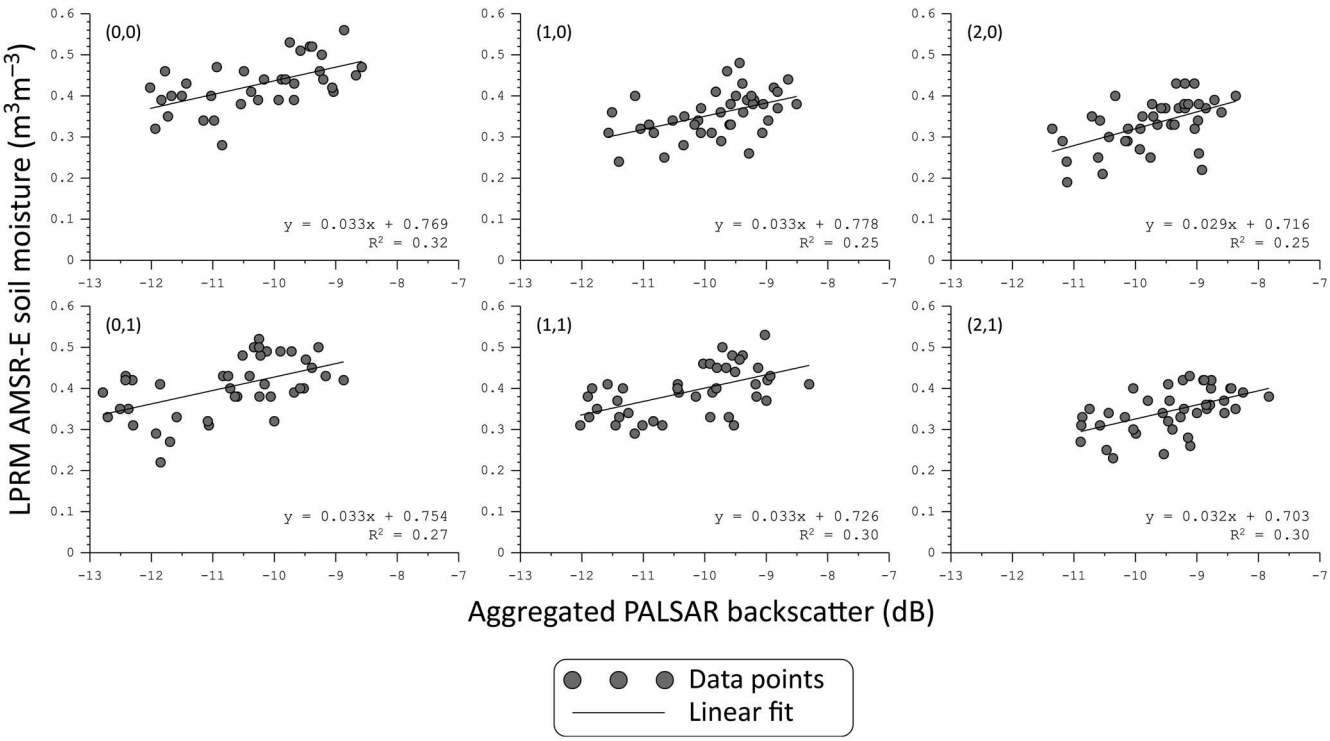

Fig. 5. LPRM AMSR-E soil moisture plotted against the normalized PALSAR σ^o aggregated to the spatial resolution of the AMSR-E product.

0.050–0.128 $m^3\ m^{-3}$ after bias correction. Nevertheless, the RMSDs remain quite large with mean values of 0.078, 0.078, and 0.079 $m^3\ m^{-3}$ for the 1-, 5- and 10-km products, respectively, and for four stations (e.g., ITCSM04, ITCSM15, ITCSM18, and ITCSM19), values even larger than 0.100 $m^3\ m^{-3}$ are found.

Specific analysis toward the nature of such large error levels reveals that for those stations, the retrievals severely

TABLE V
STATISTICS (R^2, BIAS, RMSD, MAD) COMPUTED BETWEEN THE SMAP A/P RETRIEVED SOIL MOISTURE AT 1-, 5- AND 10-KM RESOLUTION AND THE *IN SITU* MEASUREMENTS OF INDIVIDUAL STATIONS

	Retrievals at 1-km resolution				Retrievals at 5-km resolution				Retrievals at 10-km resolution			
Stations	R^2	Bias ($m^3\ m^{-3}$)	RMSD ($m^3\ m^{-3}$)	MAD ($m^3\ m^{-3}$)	R^2	Bias ($m^3\ m^{-3}$)	RMSD ($m^3\ m^{-3}$)	MAD ($m^3\ m^{-3}$)	R^2	Bias ($m^3\ m^{-3}$)	RMSD ($m^3\ m^{-3}$)	MAD ($m^3\ m^{-3}$)
ITCSM01	0.61	0.107	0.130	0.113	0.61	0.094	0.118	0.102	0.57	0.117	0.139	0.122
ITCSM02	0.56	0.271	0.277	0.271	0.52	0.251	0.259	0.251	0.46	0.279	0.286	0.279
ITCSM03	0.54	0.023	0.061	0.050	0.55	0.051	0.077	0.065	0.54	0.058	0.082	0.070
ITCSM04	0.32	0.209	0.236	0.215	0.31	0.184	0.215	0.196	0.32	0.191	0.220	0.201
ITCSM05	0.18	0.233	0.247	0.233	0.20	0.263	0.274	0.263	0.19	0.265	0.276	0.265
ITCSM06	0.44	0.208	0.218	0.208	0.56	0.169	0.178	0.169	0.54	0.170	0.180	0.170
ITCSM07	0.43	0.216	0.223	0.216	0.41	0.208	0.215	0.208	0.38	0.218	0.224	0.218
ITCSM08	0.24	0.284	0.293	0.284	0.17	0.290	0.300	0.290	0.28	0.254	0.264	0.254
ITCSM09	0.29	0.220	0.232	0.220	0.25	0.205	0.218	0.205	0.18	0.204	0.220	0.204
ITCSM10	0.42	0.085	0.114	0.091	0.39	0.106	0.132	0.110	0.40	0.123	0.146	0.124
ITCSM11	0.19	0.189	0.207	0.189	0.19	0.171	0.191	0.171	0.27	0.143	0.163	0.145
ITCSM12	0.36	0.220	0.234	0.225	0.36	0.249	0.260	0.250	0.35	0.249	0.261	0.251
ITCSM13	0.14	0.225	0.238	0.225	0.07	0.266	0.278	0.266	0.11	0.260	0.272	0.260
ITCSM14	0.17	0.033	0.069	0.056	0.20	0.044	0.074	0.059	0.16	0.086	0.103	0.091
ITCSM15	0.31	0.073	0.147	0.128	0.31	0.081	0.152	0.132	0.30	0.094	0.160	0.142
ITCSM17	0.49	0.284	0.291	0.286	0.53	0.263	0.271	0.265	0.57	0.298	0.296	0.285
ITCSM18	0.40	0.232	0.268	0.246	0.40	0.207	0.242	0.221	0.34	0.242	0.276	0.256
ITCSM19	0.56	0.119	0.191	0.158	0.52	0.117	0.192	0.158	0.42	0.139	0.211	0.178
ITCSM20	0.34	0.222	0.235	0.230	0.38	0.199	0.213	0.207	0.46	0.158	0.173	0.167
Mean	0.37	0.182	0.206	0.192	0.36	0.180	0.203	0.189	0.36	0.187	0.208	0.194
Std. Dev.	0.14	0.082	0.070	0.072	0.15	0.077	0.067	0.069	0.15	0.0672	0.065	0.066

Gray cells indicate the best performance in terms of R^2.
The mean and standard deviation values are provided at the bottom of the table.

underestimate the measurements under the wet autumn conditions. It is likely that this is related to ponding in the agricultural fields. The presence of open water within a field induces specular reflection and reduces the backscattering, while high σ^o observations are expected under wet soil conditions. Elimination of these data points from the calculations reduces the RMSD of the 1-, 5-, and 10-km products to 0.067, 0.068, and 0.069 $m^3\ m^{-3}$, respectively.

In any case, the accuracy requirement of 0.04 $m^3\ m^{-3}$ is not met even after the bias-correction. Moreover, the RMSD values obtained for the 1-, 5-, and 10-km products do typically not improve in comparison to the results from the matchup of the LPRM AMSR-E and the measured soil moisture. This is in contrast to the earlier findings of Das *et al.* [9] and Piles *et al.* [37]. Both studies report on reduced RMSDs by 0.015–0.020 $m^3\ m^{-3}$ for soil moisture retrieved at the intermediate 9-km resolution in comparison to the radiometer-only products.

Das *et al.* and Piles *et al.* made, however, use of airborne observations collected during intensive field campaigns and synthetically constructed data sets. The actual soil moisture conditions at the resolution of the retrievals are, therefore, much better defined than in this study whereby the retrievals can only be compared to measurements collected at single location. Additionally, the PALSAR σ^o and AMSR-E soil moisture combination is not ideal for demonstrating the future SMAP capabilities for several reasons. For instance, it is very likely that the SMAP L-band passive soil moisture product will outperform the AMSR-E C-band product. The PALSAR and AMSR-E instruments are also placed on the different platforms, which introduces uncertainties associated with geometry and time mismatches. Hence, the somewhat larger error statistics found in this study can be argued for. On the other hand, it is reassuring that even with this setup positive relationships with reasonably accuracy are found because calibration/validation activities by means of large scale field campaigns, such as the SMEX series (e.g., [20]), will not be feasible across the globe.

VI. DISCUSSION

In this section, the uncertainties associated with the retrieval of soil moisture from AMSR-E passive and PALSAR active microwave observations are further elaborated on. Specifically, the impact of the selected view angle correction on the retrieval accuracy is assessed and the effect of vegetation on the soil moisture sensitivity parameter β_C is investigated. Furthermore, the analysis of a series soil moisture maps is utilized to discuss the information unlocked by the downscaling of the coarse resolution passive microwave product.

A. Impact of View Angle Correction

Fig. 7 illustrates the impact of the applied view angle correction on the retrieval accuracy by showing the coefficient of determination (R^2) against the power n, defined in (3), for normalizing the PALSAR σ^o toward a reference view angle. The R^2 in the plot is calculated from five sets of soil moisture matchups whereby the retrievals are obtained with five differently normalized PALSAR σ^o data sets using n values of 1, 2, 3, 4, and 5, respectively. Since land cover is known to affect the angular response of σ^o observations, the R^2 values computed from soil moisture measured in the pastures, corn fields, and forest are presented separately. As such, the data points shown for the pastures and corn fields are averages of multiple locations, whereas the results given for the forest is based on data from a single location. Additionally, it should be noted that the presented R^2s are averages of the values obtained with the 1-, 5-, and 10-km retrievals.

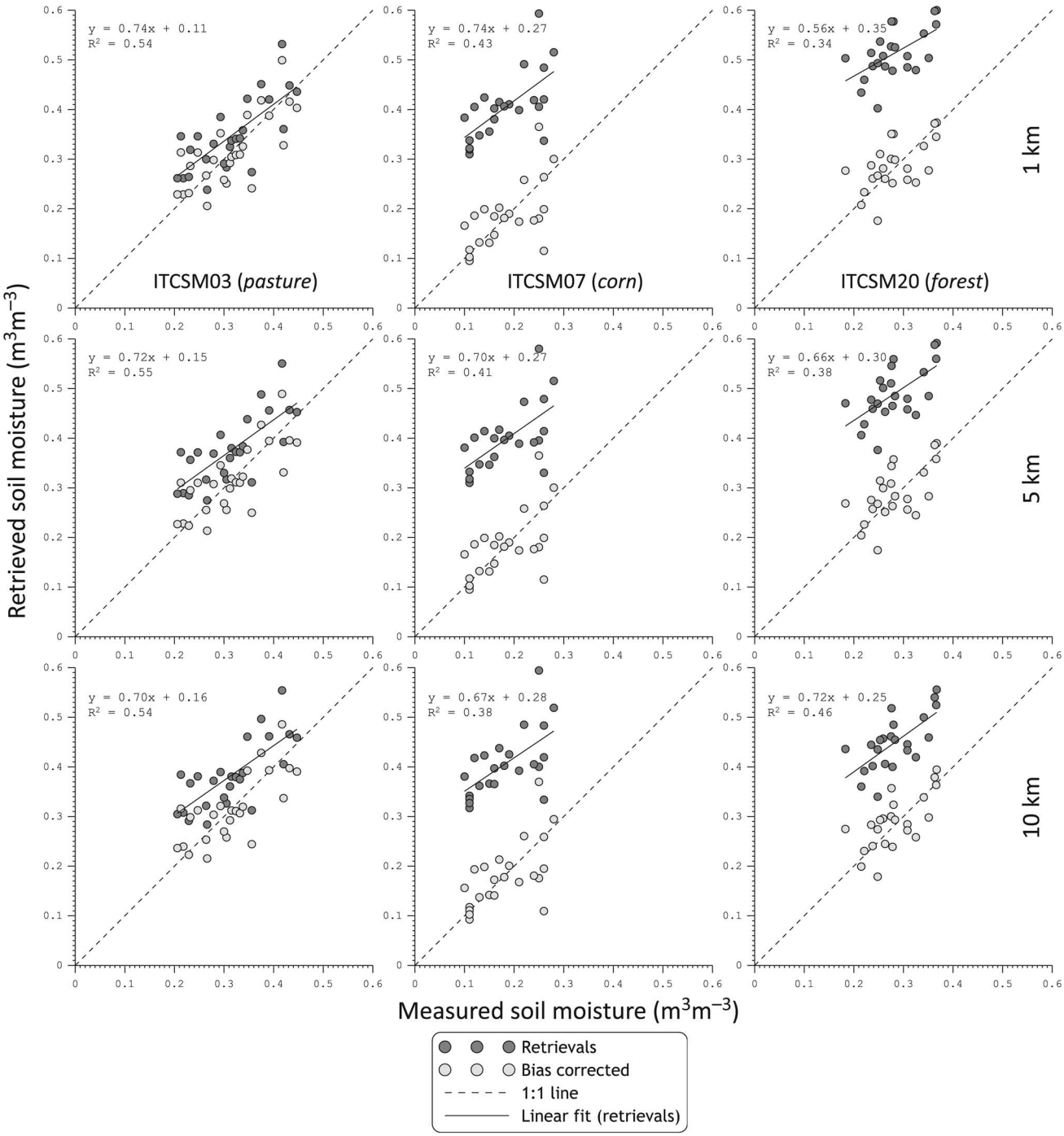

Fig. 6. Retrieved plotted against the soil moisture measured at typical corn (ITCSM09), pasture (ITCSM11), and forest (ITCSM20) sites.

The figure clearly demonstrates that the retrieval accuracy is not significantly influenced by the n value selected for the view angle normalization. The maximum R^2 range, of 0.38 to 0.43, is noted for the forest and those values are based on measurements from only a single location. For the pastures, the obtained range is negligible, and the R^2 values for the corn fields vary from 0.31 to 0.32. The notably small impact of the view angle correction on the retrieval accuracy can be explained by the fact that across a 25-km LPRM AMSR-E grid cell the nominal PALSAR view angle variation is only 3.6°. The view angle range over the entire PALSAR image swath does not affect the results because the retrieval method utilizes the difference between the σ^{o} aggregated to the coarse and intermediate resolution for the downscaling of the coarse soil moisture product.

B. *Effect of Vegetation on* β_{C}

Vegetation is known to affect both passive and active microwave observations. The LPRM considers the vegetation effect in the retrieval of soil moisture from the AMSR-E T_{b}, while the PALSAR σ^{o} is not explicitly corrected for vegetation influences. Therefore, with derivation of β_{C} from the complete

TABLE VI
RMSD AND MAD VALUES FOR THE SAME MATCHUPS AS IN TABLE IV AFTER BIAS CORRECTION

Stations	Retrievals at 1-km resolution		Retrievals at 5-km resolution		Retrievals at 10-km resolution	
	RMSD ($m^3\ m^{-3}$)	MAD ($m^3\ m^{-3}$)	RMSD ($m^3\ m^{-3}$)	MAD ($m^3\ m^{-3}$)	RMSD ($m^3\ m^{-3}$)	MAD ($m^3\ m^{-3}$)
ITCSM01	0.073	0.062	0.072	0.060	0.075	0.062
ITCSM02	0.058	0.046	0.061	0.049	0.064	0.050
ITCSM03	0.057	0.045	0.057	0.045	0.057	0.045
ITCSM04	0.110	0.087	0.110	0.087	0.110	0.088
ITCSM05	0.082	0.064	0.078	0.063	0.079	0.064
ITCSM06	0.065	0.053	0.058	0.046	0.059	0.047
ITCSM07	0.052	0.038	0.054	0.040	0.055	0.041
ITCSM08	0.072	0.060	0.077	0.064	0.070	0.057
ITCSM09	0.073	0.062	0.076	0.063	0.081	0.070
ITCSM10	0.077	0.063	0.079	0.065	0.078	0.065
ITCSM11	0.084	0.066	0.084	0.066	0.079	0.063
ITCSM12	0.078	0.055	0.077	0.056	0.078	0.057
ITCSM13	0.078	0.066	0.083	0.070	0.080	0.068
ITCSM14	0.060	0.049	0.060	0.046	0.057	0.046
ITCSM15	0.128	0.100	0.128	0.100	0.129	0.101
ITCSM17	0.053	0.044	0.053	0.045	0.073	0.050
ITCSM18	0.106	0.073	0.101	0.074	0.105	0.077
ITCSM19	0.126	0.086	0.130	0.090	0.133	0.095
ITCSM20	0.050	0.042	0.049	0.041	0.046	0.038
Mean	0.078	0.061	0.078	0.062	0.079	0.062
Std. Dev.	0.024	0.017	0.024	0.017	0.024	0.018

Gray cells indicate the resolution at which the performance in terms of both RMSD and MAD are best.

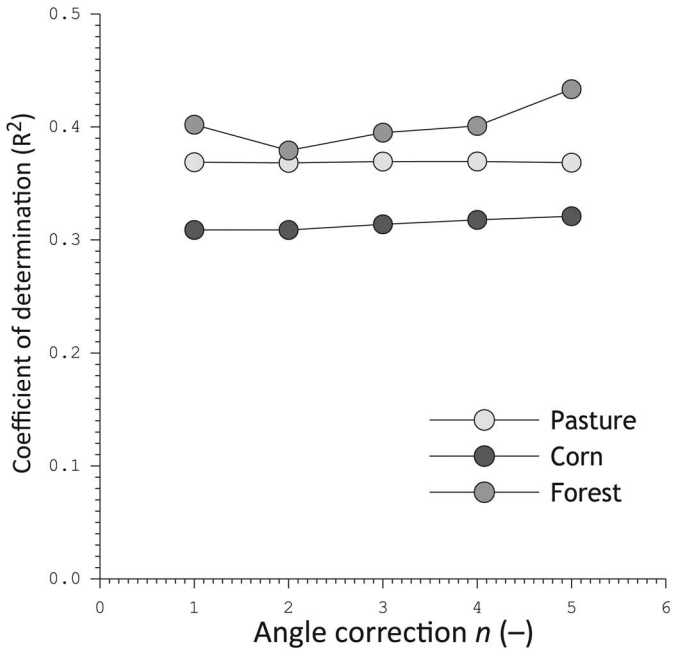

Fig. 7. Coefficients of determination computed between soil moisture measurements and retrievals obtained from downscaling the LPRM AMSR-E product using five sets of PALSAR σ^{o} normalized for the view angle with the power n of (3) for the angular correction taken equal to 1, 2, 3, 4, and 5, respectively. Results for the pasture, corn, and forest validation sites are presented separately.

set of 48 AMSR-E- PALSAR pairs, we have assumed that the vegetation effect is constant over time. This can be argued for because previous studies (e.g., [21], [22], and [24]) have provided experimental evidence for a constant σ^{o} sensitivity to soil moisture beyond intermediate vegetation biomass levels due to scattering along the soil–vegetation pathways. On the other hand, it is also known that the presence of vegetation may reduce the σ^{o} sensitivity to soil moisture.

Fig. 8 shows time series of PALSAR σ^{o}, LPRM AMSR-E and *in situ* measured soil moisture averaged for the complete study area to investigate the vegetation influences embedded within the data set. The plot illustrates that both the PALSAR σ^{o} and LPRM AMSR product capture the general soil moisture dynamics measured at the stations. Variations in the PALSAR σ^{o} match well with the *in situ* soil moisture particularly in the period from the end of May till the beginning of August. Beyond this date, the σ^{o} fluctuations cannot in every case be explained by soil moisture and also the σ^{o} response to a change in soil moisture is less than observed in the period before, which may indicate that vegetation is reducing the σ^{o} sensitivity to soil moisture. Nevertheless, the agreement found between the PALSAR σ^{o} and *in situ* soil moisture is, with an R^2 of 0.60, fairly good and considerably better than the one found between the LPRM AMSR-E soil moisture and *in situ* soil moisture measurements ($R^2 = 0.27$).

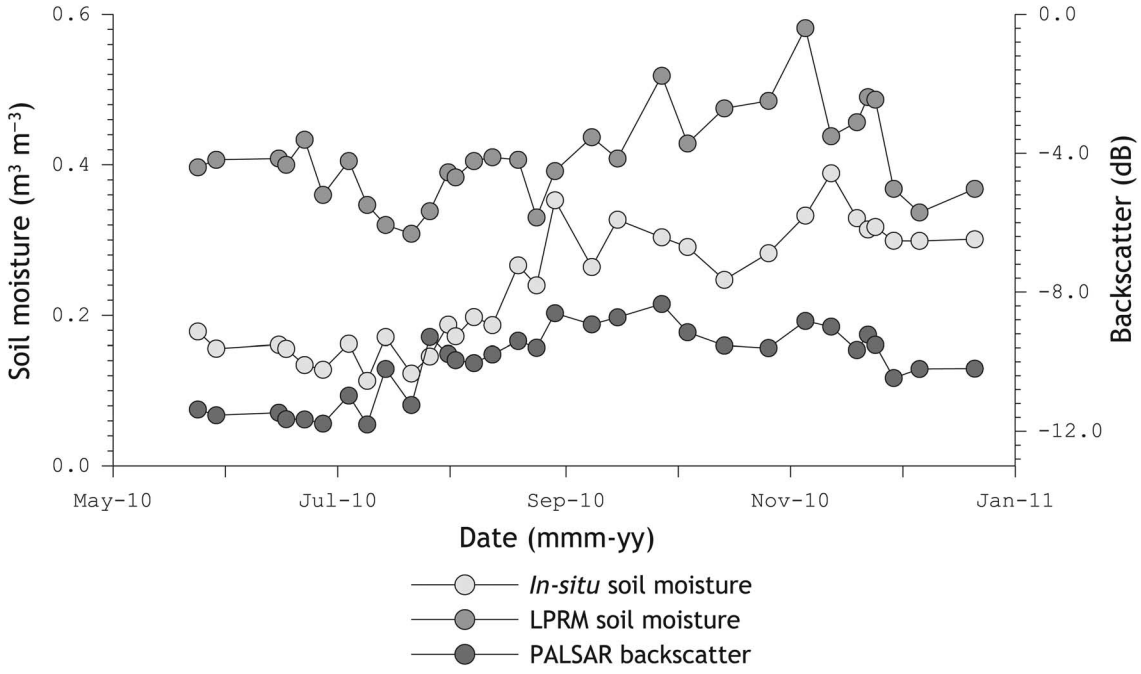

Fig. 8. Time series of PALSAR σ^{o}, LPRM AMSR-E and *in situ* measured soil moisture averaged for the complete study domain.

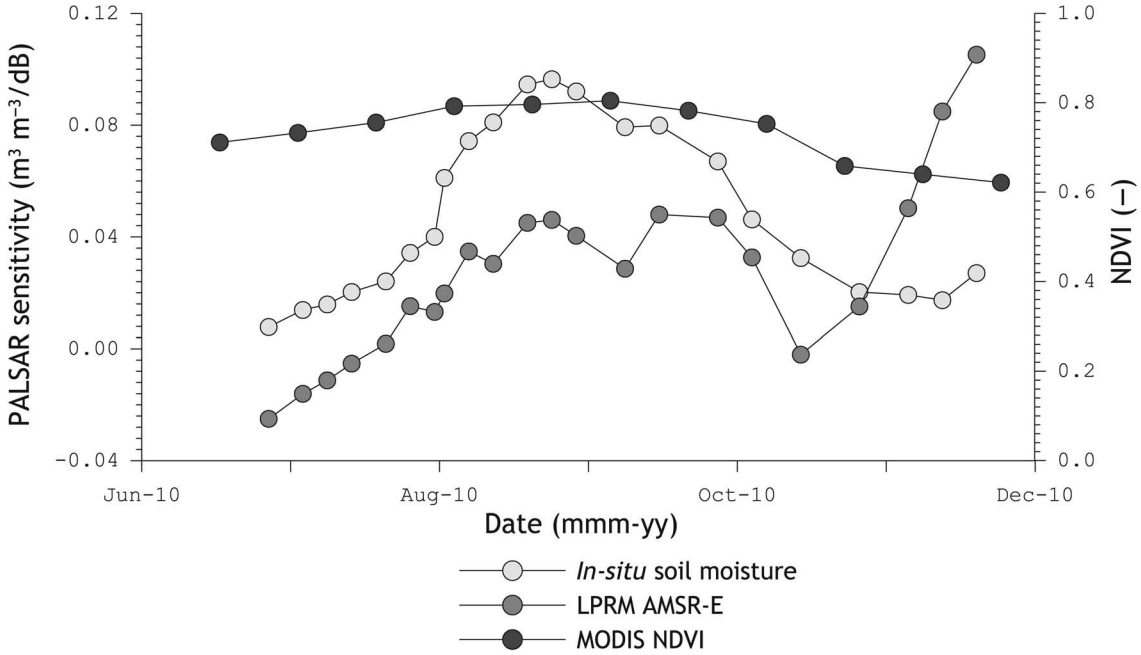

Fig. 9. PALSAR σ^{o} sensitivity to soil moisture β_{C}, calculated using PALSAR σ^{o} and soil moisture pairs from two-month gliding windows whereby both LPRM AMSR-E and *in situ* measurements are utilized as the soil moisture data source. The MODIS 16-day NDVI is shown as proxy for the vegetation conditions.

The change in the σ^{o} sensitivity to soil moisture observed along the seasons is the reason for deriving the β_{C} preferably from data collected in a period during which little changes in the vegetation conditions occur. The SMAP mission will collect active and passive microwave measurements with a 2- to 3-day revisit time and, thus, the high-temporal resolution data can be used for deriving β_{C} over short time intervals with little change in vegetation biomass; about 15–30 active/passive microwave observation pairs will be available per month. The data set available for the study area does not include a series of PALSAR images with a sufficiently high temporal resolution to make a full demonstration of this approach. As an approximation, however, a two-month gliding window is taken for calculating β_{C} from, nominal 11, PALSAR σ^{o}–soil moisture pairs.

Fig. 9 presents β_{C} computed with the LPRM AMSR-E and *in situ* measured soil moisture as a time series and the MODIS 16-day normalized difference vegetation index (NDVI) as proxy for the vegetation conditions. The little variability noted in the NDVI, from 0.62 to 0.80, is striking and may suggest that the vegetation conditions remained constant

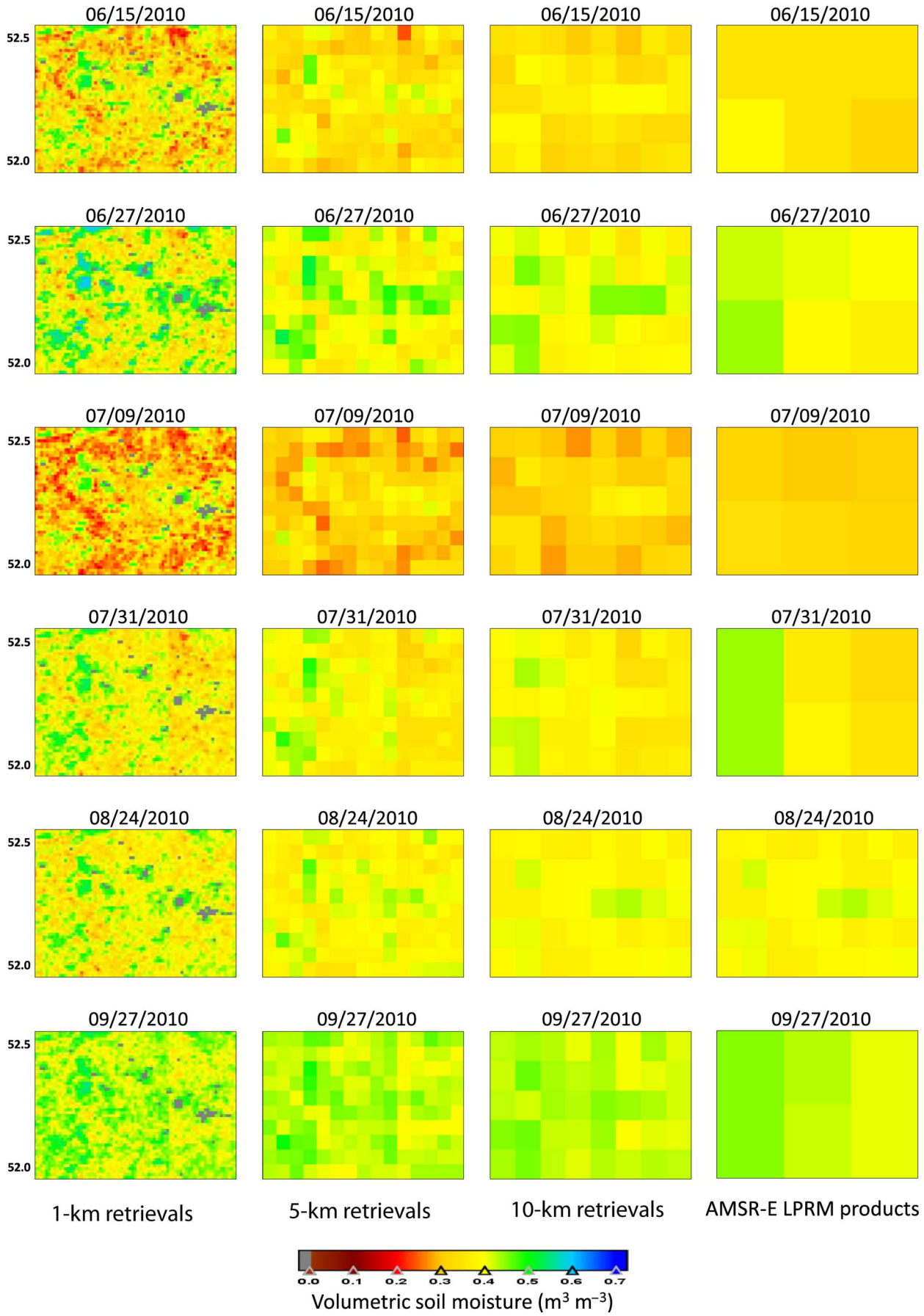

Fig. 10. Sequence of soil moisture maps obtained through application of the SMAP A/P algorithm at spatial resolutions of 1-, 5-, 10-, and 25-km resolution LPRM AMSR-E soil moisture product.

throughout the study period. This could be explained by the fact that the area is covered for more than 70% with pastures and forests that have fairly constant biomass levels across seasons. The reduced σ^{o} response to soil moisture noted in Fig. 8 from August onward could also be caused by other changes in the land surface conditions, such as an alteration in the surface roughness due to tillage practices or water standing on fields. Moreover, the largest β_{C} is calculated in the period where MODIS records the largest NDVI. This is counterintuitive and not supporting that vegetation negatively affects the magnitude of β_{C}, because for a larger vegetation biomass the sensitivity for soil moisture should decrease.

Apparently, the use of the 2-month gliding window produces ambiguous results for our data set. This is caused by the existence of prolonged dry and wet episodes within the study period. The dynamic soil moisture range measured over two months can, therefore, be small and, in those cases, uncertainties in the matchup of the PALSAR σ^{o} with soil moisture have a large impact on the determined β_{C}. As such, derivation of β_{C} from the complete set of 48 AMSR-E- PALSAR pairs is considered to provide a more robust measure for the σ^{o} sensitivity to soil moisture. The R^2 of 0.60 computed between the PALSAR σ^{o} and *in situ* measurements suggests that the vegetation effect on β_{C} is limited at least at the coarse resolution aggregation level.

C. Soil Moisture Maps

The previous sections primarily focus on the assessment of the soil moisture retrieval accuracy through comparison with measurements. However, the information content that is extracted from the resulting products will be important for the applications and science value as well. Fig. 10 shows a series of, not for bias-corrected, soil moisture maps produced at 1-, 5-, and 10-km spatial resolution and the 25-km LPRM-AMSR-E product to illustrate this.

The series of maps covers the dry spell of 2010 with its peak in the beginning of July followed up by an extremely wet September, see also Fig. 2. This sequence of a dry-down interrupted by a wet episode is well captured by Fig. 10. The spatial soil moisture variability is also in agreement with the expectations based on landscape heterogeneity, specifically at the 1-km resolution. Patterns with lower soil moisture contents develop across the cultivated regions because of a higher evaporation from the soil surface. In the areas with natural vegetation higher moisture conditions are noted, which can be expected because those top soils are undistributed and frequently covered with a thatch layer that suppresses evaporation.

However, the intensity of recorded events decreases along with the spatial resolution. For instance, the 1-km retrievals detect soil moisture levels well below 0.20 $\mathrm{m}^3\,\mathrm{m}^{-3}$ in June–July, whereas soil moisture within 5- and 10-km products barely drop below 0.25 and 0.28 $\mathrm{m}^3\,\mathrm{m}^{-3}$, respectively. This scale dependence of the information provided by soil moisture is widely acknowledged (e.g., [48]). The SMAP mission targets, therefore, to serve meteorological and hydrometeorological communities with the 36-km radiometer-only and 9-km radar/radiometer soil moisture products. Other local users (e.g., farmers and water managers) would benefit more from higher resolution soil moisture products. In this context, the development of soil moisture products from other upcoming missions with high-resolution instrumentation (e.g., Sentinel-1, PALSAR-2, and Tandem-L) could complement the SMAP mission objectives.

VII. Summary and Conclusion

In this study, soil moisture is retrieved at spatial resolutions of 1, 5, and 10 km for a 50 $\times$ 75 km study area in the east of the Netherlands using a combination of active and passive microwave observations. The selected retrieval method utilizes the passive microwave soil moisture as benchmark and employs the active microwave observations to downscale the coarse soil moisture products to an intermediate resolution. The slope of the relationship between the radar backscatter (σ^{o}) and radiometer product is adopted for downscaling, which is obtained from a series of σ^{o}-soil moisture pairs.

This downscaling approach is applied to PALSAR backscatter (σ^{o}) and VUA-NASA soil moisture product derived from C-band brightness temperatures measured by the AMSR-E. The available data set includes 48 PALSAR-AMSR-E pairs collected from May to November in the years 2008 and 2010. For validation, a network of 20 *in situ* soil moisture stations is available (operational since 2009) that is selected as one of the key validation sites for the SMAP soil moisture products.

Prior to the application of the downscaling approach, the PALSAR σ^{o} and AMSR-E soil moisture are compared to *in situ* measurements and each other. The relationships found between the PALSAR $\sigma^{\mathrm{o}}$and measured soil moisture are in agreement with previous findings. Higher σ^{o} sensitivities to soil moisture are obtained over corn fields and pastures, whereas a lower sensitivity is noted for the forest site. Also, the comparison of the VUA-NASA AMSR-E product with the measured soil moisture is in accordance with recent reports with coefficients of determination (R^2) varying from 0.09 up to 0.68. The selected AMSR-E product, however, severely overestimates the measurements by $0.18\ \mathrm{m}^3\,\mathrm{m}^{-3}$ on average, which is a well-known issue. The matchup of the aggregated PALSAR σ^{o} with the AMSR-E soil moisture results in weaker but positive relationships with R^2 of 0.25–0.32. It is also noted that the obtained σ^{o} sensitivity to the AMSR-E soil moisture is less ($0.029-0.033\ \mathrm{m}^3\,\mathrm{m}^{-3}\,\mathrm{dB}^{-1}$) as compared to the sensitivity of the PALSAR σ^{o} to the soil moisture measured at individual locations.

As a result of the overestimation by AMSR-E product, the retrievals obtained with the downscaling approach are also positively biased toward the measured soil moisture because the radiometer-only product is used as benchmark. Nevertheless, reasonable agreements are found for retrievals performed at the 1-, 5-, and 10-km resolutions with the measurements resulting in averaged R^2 values of 0.37, 0.36 to 0.36, respectively.

After bias-correction, the RMSDs calculated between the measured soil moisture and 1-, 5,- and 10-km products reach values as low as $0.046\ \mathrm{m}^3\,\mathrm{m}^{-3}$ for individual locations and are on average 0.067, 0.068, and $0.069\ \mathrm{m}^3\,\mathrm{m}^{-3}$, respectively. These

error levels do not fall within the $0.04\ \mathrm{m^3\ m^{-3}}$ error level set as accuracy requirement for satellite missions, such as the NASA soil moisture active passive (SMAP). It should, however, be noted that the PALSAR σ°-AMSR-E soil moisture combination used here is not optimum for assessment of the future capabilities of soil moisture missions. For instance, the availability of active as well as passive L-band microwave instrumentation on SMAP will greatly reduce the uncertainties that follow here from differences in view geometry, acquisition time and wavelength between PALSAR and AMSR-E. In addition, only measurements collected at a single location are available here for the assessment of the soil moisture estimates, which may not represent the actual conditions retrieved for the three respective spatial resolutions. On the other hand, soil moisture calibration/validation (Cal/Val) activities will not be able to rely on dense spatial distributions of measurements across the entire globe, such as the ones collected during the series of SMEXs. As such, this study gives a first impression on Cal/Val results that can be expected from sparsely distributed networks and in particular the Twente monitoring network.

ACKNOWLEDGMENT

The authors acknowledge the European Space Agency for providing access to the PALSAR data sets (project nr. 12031), Mr. S. Monincx from water board "Vechtstromen" for providing access to the rainfall measurements and 20 land owners of the Twente region that have made the development of soil moisture/temperature monitoring possible by granting access to their lands. Part of this research was supported by the Chinese Academy of Sciences Fellowship for Young International Scientists (Grant No. 2012Y1ZA0013).

REFERENCES

[1] M. Abdel-Messeh and S. Quegan, "Variability in ERS scatterometer measurements over land," *IEEE Trans. Geosci. Remote Sens.*, vol. 38, no. 4, pp. 1767–1776, Jul. 2000.

[2] J. Alvares-Mozos, J. Casali, M. Gonzalez-Audicana, and N. E. C. Verhoest, "Assessment of the operational applicability of RADARSAT-1 data for surface soil moisture estimation," *IEEE Trans. Geosci. Remote Sens.*, vol. 44, no. 4, pp. 913–924, Apr. 2006.

[3] J. P. Ardila, V. Tolpekin, and W. Bijker, "Angular backscatter variation in L-band ALOS ScanSAR image of Tropical Forest Areas," *IEEE Geosci. Remote Sens. Lett.*, vol. 7, no. 4, pp. 821–825, Oct. 2010.

[4] A. Berg, J. S. Famiglietti, J. P. Walker, and P. R. Houser, "Impact of bias correction to reanalysis products on simulations of North American soil moisture and hydrological fluxes," *J. Geophys. Res. Atmos.*, vol. 108, no. D16, pp. 4490, 2003.

[5] J. C. Calvet *et al.*, "Sensitivity of passive microwave observations to soil moisture and vegetation water content: L-band to W-band," *IEEE Trans. Geosci. Remote Sens.*, vol. 49, no. 4, pp. 1190–1199, Apr. 2011.

[6] N. S. Chauhan, S. Miller, and P. Ardanuy, "Spaceborne soil moisture estimation at high resolution: A microwave-optical/IR synergistic approach," *Int. J. Remote Sens.*, vol. 24, no. 22, pp. 4599–4622, Nov. 2003.

[7] N. S. Chauhan, D. M. Le Vine, and R. H. Lang, "Discrete scatter model for microwave radar and radiometer responses to corn: Comparison of theory and data," *IEEE Trans. Geosci. Remote Sens.*, vol. 32, no. 2, pp. 416–426, Mar. 1994.

[8] W. T. Crow *et al.*, "Upscaling sparse ground-based soil moisture observations for the validation of coarse-resolution satellite soil moisture products," *Rev. Geophys.*, vol. 50, p. RG2002, 2012.

[9] N. N. Das, D. Entekhabi, and E. G. Njoku, "An algorithm for merging SMAP radiometer and radar data for high-resolution soil-moisture retrieval," *IEEE Trans. Geosci. Remote Sens.*, vol. 49, no. 5, pp. 1504–1512, May 2011.

[10] N. N. Das *et al.*, "Tests of the SMAP combined radar and radiometer algorithm using airborne field campaign observations and simulated data," *IEEE Trans. Geosci. Remote Sens.*, vol. 52, no. 4, pp. 2018–2028, Apr. 2014.

[11] L. Dente, Z. Su, and J. Wen," Validation of SMOS soil moisture products over the Maqu and Twente regions," *Sensors*, vol. 12, pp. 9965–9986, 2012.

[12] M. C. Dobson and F. T. Ulaby, "Preliminary evaluation of the SIR-B response to soil moisture, surface roughness, and crop canopy cover," *IEEE Trans. Geosci. Remote Sens.*, vol. GE-24, no. 4, pp. 517–526, Jul. 1986.

[13] S. Draper, J. P. Walker, P. J. Steinle, R. A. M. de Jeu, and T. R. H. Holmes, "An evaluation of AMSR–E derived soil moisture over Australia," *Remote Sens. Environ.*, vol. 113, pp. 703–710, 2009.

[14] D. Entekhabi *et al.*, "The soil moisture active passive (SMAP) mission," *Proc. IEEE*, vol. 98, no. 5, pp. 704–716, May 2010.

[15] J. S. Famiglietti *et al.*, "Ground-based investigation of soil moisture variability within remote sensing footprints during the Southern Great Plains 1997 (SGP97) hydrology experiment," *Water Resour. Res.*, vol. 35, no. 6, pp. 1839–1851, Jun. 1999.

[16] P. Ferrazzoli and L. Guerriero, "Radar sensitivity to tree geometry and woody volume: A model analysis," *IEEE Trans. Geosci. Remote Sens.*, vol. 33, no. 2, pp. 360–371, Mar. 1995.

[17] A. K. Fung, Z. Li, and K. S. Chen, "Backscattering from a randomly rough dielectric surface," *IEEE Trans. Geosci. Remote Sens.*, vol. 30, no. 2, pp. 356–369, Mar. 1992.

[18] C. Gruhier *et al.*, "Soil moisture active and passive microwave products: Intercomparison and evaluation over a Sahelian site," *Hydrol. Earth Syst. Sci.*, vol. 14, pp. 141–156, 2010.

[19] T. J. Jackson, "Measuring surface soil moisture using passive microwave remote sensing," *Hydrol. Processes*, vol. 7, no. 2, pp. 139–152, 1993.

[20] T. J. Jackson *et al.*, "Validation of advanced microwave scanning radiometer soil moisture products," *IEEE Trans. Geosci. Remote Sens.*, vol. 48, no. 12, pp. 4256–4272, Dec. 2010.

[21] A. T. Joseph, R. van der Velde, P. E. O'Neill, R. Lang, and T. Gish, "Effects of corn on C- and L-band radar backscatter: A correction method for soil moisture retrieval," *Remote Sens. Environ.*, vol. 114, pp. 2417–2430, 2010.

[22] A. T. Joseph, R. van der Velde, P. E. O'Neill, R. Lang, and T. Gish, "Soil moisture retrieval during a corn growth cycle using L-band (1.6 GHz) radar observations," *IEEE Trans. Geosci. Remote Sens.*, vol. 46, no. 8, pp. 2365–2374, Aug. 2008.

[23] Y. H. Kerr *et al.*, "Soil moisture retrieval from space: The soil moisture and ocean salinity (SMOS) mission," *IEEE Trans. Geosci. Remote Sens.*, vol. 39, no. 8, pp. 1729–1735, Aug. 2001.

[24] Y. Kim and J. J. van Zyl, "A time-series approach to estimate soil moisture using polarimetric radar data," *IEEE Trans. Geosci. Remote Sens.*, vol. 47, no. 8, pp. 2519–2527, Aug. 2009.

[25] H. Lievens *et al.*, "Effective roughness modelling as a tool for soil moisture retrieval from C-and L-band SAR," *Hydrol. Earth Syst. Sci.*, vol. 15, pp. 151–162, 2011.

[26] A. Loew, R. Ludwig, and W. Mauser, "Derivation of surface soil moisture from ENVISAT ASAR wide swath and image mode data in agricultural areas," *IEEE Trans. Geosci. Remote Sens.*, vol. 44, no. 4, pp. 889–899, May 2006.

[27] O. Merlin *et al.*, "Disaggregation of SMOS soil moisture in Southeastern Australia," *IEEE Trans. Geosci. Remote Sens.*, vol. 50, no. 5, pp. 1556–1571, May 2012.

[28] O. Merlin, J. P. Walker, A. Chehbouni, and Y. Kerr, "Towards deterministic downscaling of SMOS soil moisture using MODIS derived soil evaporative efficiency," *Remote Sens. Environ.*, vol. 112, pp. 3935–3946, 2008.

[29] V. L. Mironov, L. G. Kosolapova, and S. V. Fomin, "Physically and mineralogically based spectroscopic dielectric model for moist soils," *IEEE Trans. Geosci. Remote Sens.*, vol. 47, no. 7, pp. 2057–2070, Jul. 2009.

[30] I. E. Mladenova, T. J. Jackson, R. Bindlish, and S. Hensley, "Incidence angle normalization of radar backscatter data," *IEEE Trans. Geosci. Remote Sens.*, vol. 51, no. 3, pp. 1791–1804, Mar. 2013.

[31] U. Narayan, V. Lakshmi, and T. J. Jackson, "High-resolution change estimation of soil moisture using L-band radiometer and radar observations made during the SMEX02 experiments," *IEEE Trans. Geosci. Remote Sens.*, vol. 44, no. 6, pp. 2659–2673, Jun. 2006.

[32] G. Njoku *et al.*, "Observations of soil moisture using a passive and active low-frequency microwave airborne sensor during SGP99," *IEEE Trans. Geosci. Remote Sens.*, vol. 40, no. 12, pp. 2659–2673, Dec. 2002.

[33] G. Njoku and D. Entekhabi, "Passive microwave remote sensing of soil moisture," *J. Hydrol.*, vol. 184, pp. 101–129, 1996.

[34] P. E. O'Neill, N. S. Chauhan, and T. J. Jackson, "Use of active and passive microwave remote sensing for soil moisture estimation through corn," *Int. J. Remote Sens.*, vol. 17, no. 10, pp. 1851–1865, 1996.
[35] M. Owe, R. A. M. de Jeu, and J. P. Walker, "A methodology for surface soil moisture and vegetation optical depth retrieval using the microwave polarization difference index," *IEEE Trans. Geosci. Remote Sens.*, vol. 39, no. 8, pp. 1643–1654, Aug. 2001.
[36] M. Owe, R. A. M. de Jeu, and T. Holmes, "Multisensor historical climatology of satellite-derived global land surface moisture," *J. Geophys. Res.*, vol. 113, p. F01002, 2008, doi: 10.1029/2007JF000769.
[37] M. Piles, D. Entekhabi, and A. Camps, "A change detection algorithm for retrieving high-resolution soil moisture from SMAP radar and radiometer observations," *IEEE Trans. Geosci. Remote Sens.*, vol. 47, no. 12, pp. 4125–4131, Dec. 2009.
[38] M. Piles *et al.*, "Downscaling SMOS-derived soil moisture using MODIS visible/infrared data," *IEEE Trans. Geosci. Remote Sens.*, vol. 49, no. 9, pp. 3156–3166, Sep. 2011.
[39] S. Saatchi, K. Halligan, D. G. Despain, and R. L. Crabtree, "Estimation of forest fuel load from radar remote sensing," *IEEE Trans. Geosci. Remote Sens.*, vol. 45, no. 6, pp. 1726–1740, Jun. 2007.
[40] T. J. Schmugge, W. P. Kustas, J. C. Ritchie, T. Jackson, and A. Rango, "Remote sensing in hydrology," *Adv. Water Resour.*, vol. 25, pp. 1367–1385, 2002.
[41] M. Shimada, O. Isoguchi, T. Tadono, and K. Isono, "PALSAR radiometric and geometric calibration," *IEEE Trans. Geosci. Remote Sens.*, vol. 47, no. 12, pp. 3915–3932, Dec. 2009.
[42] Z. Su *et al.*, "The Tibetan Plateau observatory of plateau scale soil moisture and soil temperature (Tibet-Obs) for quantifying uncertainties in coarse resolution satellite and model products," *Hydrol. Earth Syst. Sci.*, vol. 15, pp. 2303–2316, 2011.
[43] D. P. Thoma *et al.*, "Appropriate scale of soil moisture retrieval from high resolution radar imagery for bare and minimally vegetated soils," *Remote Sens. Environ.*, vol. 112, no. 2, pp. 403–414, 2008.
[44] F. T. Ulaby, R. K. Moore, and A. K. Fung, "Microwave remote sensing: Active and passive," in *Radar Remote Sensing and Surface Scattering and Emission Theory*, vol. 2. Reading, MA, USA: Addison-Wesley, 1982.
[45] R. van der Velde, Z. Su, and Y. Ma, "Impact of soil moisture dynamics on ASAR σ^{o} signatures and its spatial variability observed over the Tibetan Plateau," *Sensors*, vol. 8, pp. 5479–5491, 2008.
[46] R. van der Velde *et al.*, "Soil moisture mapping over the central part of the Tibetan Plateau using a series of ASAR WS images," *Remote Sens. Environ.*, vol. 120, pp. 175–187, 2012a.
[47] R. van der Velde, M. S. Salama, M. D. van Helvoirt, Z. Su, and Y. Ma, "Decomposition of uncertainties between coarse MM5–Noah-simulated and fine ASAR-retrieved soil moisture over central Tibet," *J. Hydrometeorol.*, vol. 13, pp. 1925–1938, Dec. 2012.
[48] K. Y. Vinnikov, A. Robock, N. A. Speraskaya, and C. A. Schlosser, "Scales of temporal and spatial variability of midlatitude soil moisture," *J. Geophys. Res.*, vol. 101, no. D3, pp. 7163–7174, Mar. 1996.
[49] W. Wagner, G. Lemoine, M. Borgeaud, and H. Rott, "A study of vegetation cover effects on ERS scatterometer data," *IEEE Trans. Geosci. Remote Sens.*, vol. 37, no. 2, pp. 938–948, Mar. 1999.
[50] W. Wagner, V. Naeimi, K. Scipal, R. A. M. de Jeu, and J. Martínez-Fernández, "Soil moisture from operational meteorological satellites," *Hydrogeol. J.*, vol. 15, pp. 121–131, 2007.
[51] I. H. Woodhouse, *Introduction to Microwave Remote Sensing*. Boca Raton, FL, USA: CRC Press, 2005.

Rogier van der Velde received the M.Sc. degree in hydrology from Wageningen University, Wageningen, The Netherlands, and the Ph.D. degree in soil moisture remote sensing and land surface hydrology from the University of Twente, Enschede, The Netherlands.

Since 2010, he has been an Assistant Professor of Earth Observation and Land Surface Hydrology with the Faculty of Geo-Information Science and Earth Observation (ITC), University of Twente. His research interests include soil moisture estimation from active as well as passive microwave observation for the understanding of hydrometeorological processes.

M. Suhyb Salama received the B.Sc. degree in civil engineering from Damascus University, Damascus, Syria, in 1993, and the M.Sc. degree with Great Distinction in hydraulic engineering and the Ph.D. degree in civil engineering both from Katholieke Universiteit Leuven, Leuven, Belgium, in 1999 and 2003, respectively.

Currently, he is an Associate Professor with the Faculty of Geo-information Science and Earth Observation (ITC), the University of Twente, Enschede, The Netherlands. He is also the Director of Smart Hydrology, a private firm pioneering the state-of-the-art GEO-ICT solutions to safeguard water resources. His research interests include remote sensing and numerical modeling of hydrology and interactions with the ecosystem.

Omar Ali Eweys was born in Giza, Egypt, on March 1, 1982. He received the B.Sc. degree in soil sciences from Cairo University, Giza, Egypt, in 2004, the M.Sc. degree in physical land resources from Ghent University, Ghent, Belgium, in 2009, and the Postgraduate Diploma in geoinformation science and earth observation from Twente University, Enschede, The Netherlands, in 2011. Currently, he is pursuing the Ph.D. degree at the Faculty of ITC, Twente University focused on optimizing irrigation water management using satellite observed soil moisture.

He is an Assistant Lecturer with the Faculty of Agriculture, Cairo University.

Jun Wen received the B.Sc. degree in meteorology from Peking University, Beijing, China, and the M.Sc. and Ph.D. degrees in meteorology from Atmospheric Physics Division, Chinese Academy of Sciences, Beijing, China.

From 2000 to 2002, he did the Postdoctoral research at Wageningen University, Wageningen, The Netherlands. From 2002 to 2003, he was a Visiting Scientist with the Hydrology and Remote Sensing Laboratory, USDA-ARS. Since 2004, he has been a Professor of Land Surface Process and Climate Change with the Key Laboratory of Land Surface Process and Climate Change in Cold and Arid Regions, Chinese Academy of Sciences, Beijing, China.

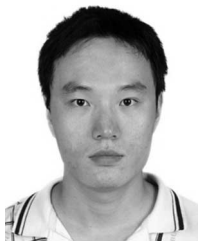

Qiang Wang was born in Shanxi, China, on July 13, 1986. He received the B.S. degree in geodesy in 2008 and pursued a combined M.Sc./Ph.D. degrees in synthetic aperture radar interferometry both at the China University of Mining and Technology, Beijing, China. Since 2014, he has been pursuing the Ph.D. degree in soil moisture estimation using a combination of active and passive microwave remote sensing at the Department of Water Resources, Faculty of ITC, University of Twente, Enschede, The Netherlands.

His research interests include combining active and passive microwave remote sensing to retrieve soil moisture over the Tibetan Plateau.